Proceedings of ASME Turbo Expo 2011
GT2011
June 6-10, 2011, Vancouver, British Columbia, Canada

GT2011-45592

RADIATION EFFECTIVENESS ON THE AERO- AND THERMODYNAMICS IN A HIGHLY THERMALLY LOADED FILM COOLING SYSTEM

Wang Wenping Sun Peng Ren Jing Jiang Hongde
Institute of Power Mechanics and Engineering
Dept. of Thermal Engineering, Tsinghua University
Beijing, 100084, China

ABSTRACT

With the increasing of the gas turbine inlet temperature, the radiative heat transfer plays a more important role in the total heat transfer. In this paper, a high temperature test rig has been built to research the radiative effect in high temperature film cooling. The test section is made up of a high temperature hot gas channel and a middle temperature coolant air channel which are separated by a flat plate with a row of film cooling holes. The goal is to analyze the effects of radiation and its interaction between conduction and convection in the internal and film cooling which consider the heat transfer in both gas and solid. Meanwhile, the numerical study on the test cases are also carried out by combining conjugate heat transfer with radiative models. The fluid and solid regions were solved simultaneously. The Discrete Ordinates (DO) model and the Weighted Sum of Gray Gases Model (WSGGM) has been used to solve the radiative transfer equation for the radiation modeling. The results show that the temperature of the plate increase greatly when the radiation is taken into account and the temperature gradient through the plate becomes much larger. The temperature distribution has been changed and become smoother in spanwise direction. The results also indicate that the internal emissivity of the inlet has an influence mainly on the whole temperature of the plate, which suggests that the control of inlet emissivity is a good way for prevent over-high temperature on the first stage gas turbine vane.

INTRODUCTION

Increasing gas temperature is an important way to enhance the performance of gas turbine. The working temperature at the advanced gas turbine inlet are much higher than the material could stand, which leads to the necessity of higher temperature endurance of the material, the more advanced techniques of thermal barrier coating, and the more efficient cooling system for a long service life. A good prediction on the distribution of some characteristics such as flow field, heat transfer and structure intensity inside the high temperature turbine is profitable for the designing and manufacturing of the turbine blade.

With the increase of the turbine inlet temperature, the radiative heat transfer increases as a fourth power, which leads to a huge and unneglectable radiative intensity at the inlet of the first stage. Understanding the effects of radiation in the heat transfer and the interaction between radiation and the other two heat transfer methods is an essential component in developing efficient and effective cooling strategies when the turbine is working in high temperature environment.

Many researchers have studied the effects on radiative heat transfer. Kumar and Kale [1] studied the conjugate heat transfer in a two-dimensional blade by a FEM based numerical scheme. The convective heat transfer was modeled by assuming constant free stream temperature and a local average heat transfer coefficient which varies along the surfaces, and constant temperature and heat transfer coefficient at the coolant side. The radiation was simplified by modeling the radiation environment as an all enclosing large surface whose temperature is constant. The results showed a decrease of radiative heat transfer when TBC was used. He and Tan, et al. [2] employed the discrete ordinates model in general body fitted coordinates to simulate radiation in a three dimensional vane channel of engine with an already known flow and temperature field. The numerical simulation indicated that incident radiative heat fluxes increase from 188% to 212% when temperature of inlet gas increase 29.9%. Zhang and Liu, et al. [3] established a coupled flow-thermal model to analyze the conjugate heat transfer of 3D turbine blade. The radiation was solved with P-1 model. The results showed that when the gas temperature was high, the blade surface temperature increased greatly, and led to quite different temperature distribution by considering the radiation. Mazzotta and Alvin [4] studied the temperature distribution on a 2D E3 airfoil at the turbine inlet temperature exceeding 1700°C with different gas compositions, P-1 model was employed to solve the radiative heat transfer equation. Results showed the contribution of radiation on the total surface heat flux was up to 5.7%. Akwaboa, Mensah, and Diwan[5] focuses on the combined effects of radiation and conduction heat transfer in the semitransparent TBCs, they showed that by taking into account the effect of radiation, the temperature distribution in the metal substrate with TBC exceeded the that without radiation by about 40 K, signifying the importance of including radiation in the thermal modeling of TBCs for high temperature applications.

In experimental aspects, Bohn, et al. [6] used a high-enthalpy wind tunnel to produce stationary air flows with static temperatures between 2000 K and 3000 K and velocities varied between Ma = 0.5 and Ma = 1. The cooling efficiency related on the density and velocity ratios were measured and analyzed. In University of Pittsburgh, a high temperature, pressurized aerothermal test facility was built to experimentally characterize aerothermal heat transfer for advanced turbine applications using TBC-coated and uncoated superalloy test coupons exposed to combustion gas temperatures & chemistries. The design & construction of the experimental test module has completed [7].

In this paper, a high temperature test rig made up by a flat plate with a row of film cooling holes put in hot gas at about 800°C and coolant air at about 400°C has been built to study the theory of the combination of conduction, convection and radiation, i.e. the conjugate heat transfer. The effect of conjugate heat transfer between conduction and convection are studied in [8] and showed the adverse effect of the hot gas entrainment smeared out due to the conduction and the convection of the coolant side which made the temperature distribution smoother on the top surface. In this paper both experimental and numerical methods are employed to understand the effects of radiation in the heat transfer and the interaction between radiation and the other two heat transfer methods.

DESCRIPTION OF THE TEST RIG

The high temperature film cooling test rig is showed in figure 1 and figure 2 is the sketch map. The test rig is composed of the hot gas supply system, the coolant air supply system, the flat plate test section, the exhaust section and the measuring instruments.

The hot gas and the coolant air supply systems

The heart of the hot gas supply system is a 380 Mcal/h burner, used to produce high temperature gas by combustion. In the burner, the primary air is mixed with the Liquid Petrol Gas (LPG) fuel and then ignited by a high voltage spark type igniter plug. The igniter will work for several seconds till the combustion process becomes self sustaining. The fuel flowrate can be adjusted from 15 to 30 kg per hour to adjust the burner output power at a range of 200~400 Mcal/h. The flowrate of the primary air is adjusted in accordance with the fuel.

The combustion product leaving the burning section, which has a temperature about 2000°C, will enter the diluting section and then mix with the diluting air supplied by the top blower and the extra steam supplied by the water supply system.

Figure 1. PHOTO OF THE TEST RIG

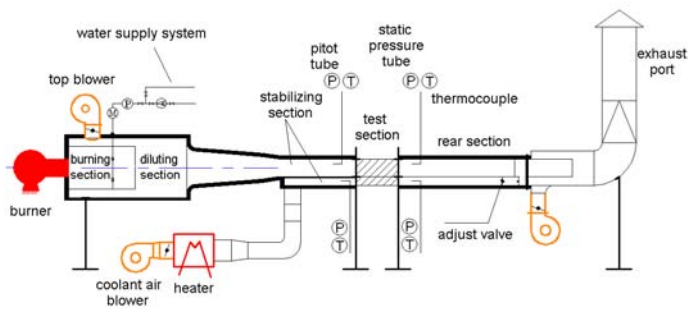

Figure 2. SKETCH MAP OF THE TEST RIG

The water supply system is used to adjust the hot gas composition. The water is delivered into the diluting section through eight atomization nozzles, which are spaced equally around the diluting section. The flowrate of the water go through one nozzle can be controlled by the water pressure, as showed in figure 3. The water is vaporized in the diluted section because of the high temperature and then mixed with the combustion gas and the diluting air to generate the 800°C hot gas which goes through the stabilizing channel into the hot gas channel of the test section.

The coolant air is generated by another blower and an 80kW electric heater. The power of the heater and the flowrate of the blower can be adjusted self-adaptively, which makes the air temperature stable at about 400°C. Then the air goes through a long stabilizing channel into the coolant air channel of the test section. The maximum flowrate can reach 500 Nm^3/h, i.e. 500 m^3/h at 0°C, 1atm.

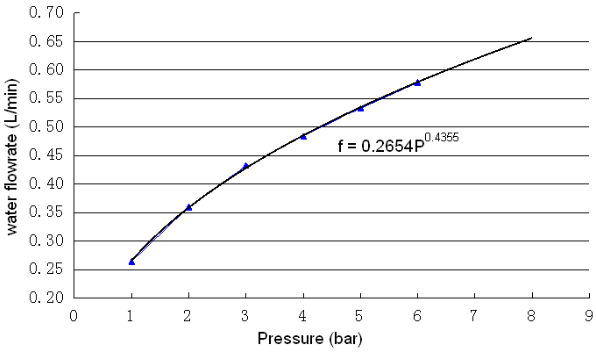

Figure 3. THE CALIBRATION CURVE OF ONE ATOMIZATION NOZZLE

The flat plate test section

The test section is the main part for data acquisition. It is composed of two channels, the 800°C hot gas goes through the upper channel while the 400°C coolant air goes through the lower. All the parts ahead of the test section are separated and wrapped by the fiberglass batt, a type of heat insulated material, so the hot gas and the coolant air have no interaction until they reach the test section.

The test section is a simplified model of a part of the leading edge of the first stage gas turbine vane where both the film cooling and the internal cooling exist, and the incident radiation of the combustor take effects. As showed in figure 4, the hot gas channel and the coolant air channel are separated by a nickel-based superalloy flat plate, which has the thickness of 18 mm. There are five film cooling holes on the plate, the diameters of the holes are d = 8 mm, the distance between each two adjacent holes are 3d and the inclination angle is α = 35°. The length of the plate is 423 mm (about 52d) and the width is 206mm (about 25d). The outlets of the film cooling holes are 10d from the front of the plate. The test section are also wrapped by the heat insulated material to prevent heat transfer between the test section and the environment (figure 5).

When the test rig runs, the hot gas and coolant air will go through their channels at a speed of 15~20 m/s. An adjust valve is installed in the coolant air channel after the test section to make the back pressure of the coolant air channel higher than that of the hot gas channel by decreasing the flow area of the coolant air channel. Due to the pressure difference, the coolant air will go to the hot gas channel through the film cooling holes and mix with the hot gas, which forms the film cooling. Different pressure difference can be adjusted by the valve to obtain different blowing ratios. Meanwhile, as the thermal conductivity of the plate is not low, heat transfer takes place from hot gas to coolant air through the plate, which forms the internal cooling.

When the hot gas and the coolant air go out of the test section, they go through the rear section to exhaust to the atmosphere. The adjust valve is installed in the rear section.

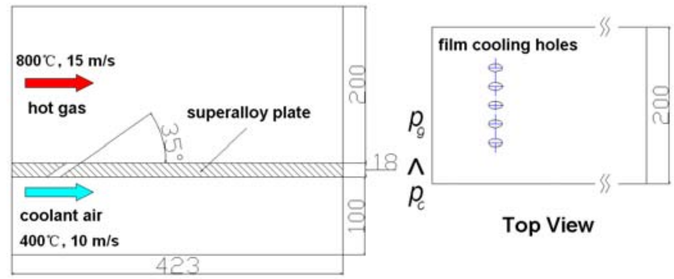

Figure 4. SKETCH MAP OF THE TEST SECTION

Figure 5. PHOTO OF THE TEST SECTION (WRAPPED AND NOT WRAPPED)

The measuring instruments

The main instruments for measuring are the thermal couples, the pitot tubes, the static pressure tubes, the chromatographic analyzer and the PIV technique.

Four armoured thermocouples are set at the center of the hot gas and the coolant air channels before and after the test section to measure the temperatures of the inflow and the outflow. Two pitot tubes are located at the center of each channel before the test section to get the velocities of the inflow, while the back pressures of the channels are acquired by the static pressure tubes located after the test section.

In the test section, ten thermocouples are embedded on the top and bottom surfaces of the flat plate in order to measure the surface temperature. They are located along the centerlines of the middle film cooling hole streamwisely. The detail of the position of the thermocouples is listed in table 1 and figure 6.

There is a gas collecting tube located at the hot gas channel of the stabilizing section. The composition of the hot gas is obtained using the chromatographic analyzer from the sample collected during the experiment. And PIV technique is used to observe the flow field.

The uncertainty of the thermocouple is 0.3%, and the chromatographic analyzer is 2.2%. The correction factors of the pitot tubes and the static tubes are calibrated to be unity. The uncertainty of the whole test system is calculated to be 2.3%.

Table 1. The position of the thermocouples

top surface	A1	A2	A3	A4	A5
to the rear of holes	1 *d*	2 *d*	5 *d*	10 *d*	17 *d*
bottom surface	B1	B2	B3	B4	B5
to the rear of holes	0.75 *d*	2.25 *d*	5 *d*	10 *d*	17 *d*

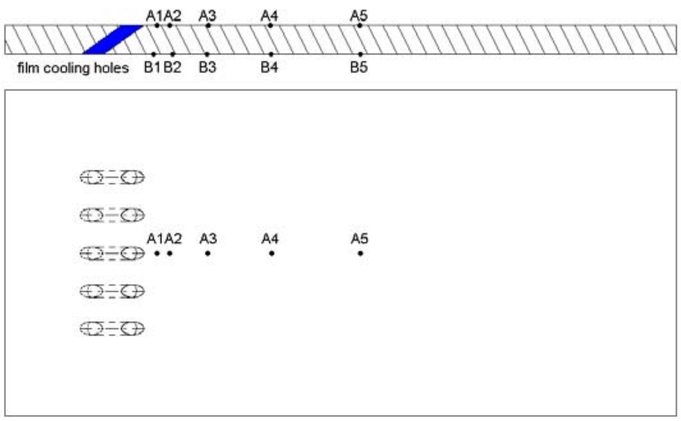

Figure 6. THE POSITION OF THE THERMOCOUPLES

NUMERICAL SCHEME

The numerical study is employed to see the details of the radiative effect and its interaction with conductive and convective heat transfer. The computational result is first compared with the experimental data to validate the numerical method, then the further investigations will be discussed.

DO model is employed to solve the radiative heat transfer equation and WSGGM is used to determine the absorption coefficient of the gas.

The Discrete Ordinate radiation model

In the numerical study, the fluid region and the solid region are solved simultaneously, i.e. the conjugate heat transfer method is used in energy transport. For the radiation, the Discrete Ordinate model is employed into the numerical scheme.

The Discrete Ordinate model solves the radiative transfer equation for a finite number of discrete solid angles, each associated with a direction vector $\vec{s}$ fixed in the global Cartesian system.

The governing equation of the radiative transfer for a gray medium in the direction $\vec{s}$ is:

$$\frac{\mathrm{d}\, I(\vec{r},\vec{s})}{\mathrm{d}\, s} + (a+\sigma_s) I(\vec{r},\vec{s}) = an^2\frac{\sigma T^4}{\pi} + \frac{\sigma_s}{4\pi}\int_0^{4\pi} I(\vec{r},\vec{s}\,')\Phi(\vec{s}\cdot\vec{s}\,')d\Omega' \quad (1)$$

where I is the radiative intensity, $\vec{r}$ is the position vector, $\vec{s}$ is the direction vector, $\vec{s}\,'$ is the scattering direction vector, s is the path length in the direction $\vec{s}$, a is the absorption coefficient of the medium, σ_s is the scattering coefficient, n is the refractive index, Φ is the scattering phase function, and Ω' is the solid angle.

The DO model considers the radiative transfer equation in the direction $\vec{s}$ as a field equation, thus equation (1) could be written as:

$$\nabla\cdot I(\vec{r},\vec{s})\vec{s} + (a+\sigma_s) I(\vec{r},\vec{s}) = an^2\frac{\sigma T^4}{\pi} + \frac{\sigma_s}{4\pi}\int_0^{4\pi} I(\vec{r},\vec{s}\,')\Phi(\vec{s},\vec{s}\,')d\Omega' \quad (2)$$

The DO model assumes the radiative intensity in one solid angle is equal, thus the integral part in equation (2) could be substituted by the sum of some finite discrete values. In Cartesian coordinates, equation (2) could be written as:

$$\xi_i\frac{\partial I}{\partial x_i} + (a+\sigma_s)I = an^2\frac{\sigma T^4}{\pi} + \frac{\sigma_s}{4\pi}\sum_{j=1}^{N\Omega} w_j I_j \Phi_j \quad (3)$$

where ξ_i is the direction cosine of the direction vector $\vec{s}$, w_j is the weight factor of the radiative intensity in the scattering direction $\vec{s}_i$, $N\Omega$ is the number of the total discrete solid angles in the space.

When the boundary is gray-diffuse, the radiative intensity on the boundary could be written as:

$$I_w = \frac{1-\varepsilon}{\pi}\int_{\vec{s}\cdot\vec{n}>0} I(s)\vec{s}\cdot\vec{n}\,d\Omega + \frac{\varepsilon\sigma T_w^4}{\pi} \quad (4)$$

where $\vec{n}$ is the unit surface vector normal pointing out of the domain, T_w is the boundary temperature and ε is its emissivity.

In energy equation:

$$\frac{\partial}{\partial t}(\rho E) + \nabla\cdot(\vec{v}(\rho E+p)) = \nabla\cdot(k_{eff}\nabla T + (\tau_{eff}\cdot\vec{v})) + S_h \quad (5)$$

The radiative contribution to the source term S_h could be written as:

$$S_h^r = a\int_{4\pi}(I(\vec{r},\vec{s}) - I_b(\vec{r}))d\Omega \quad (6)$$

where the superscript r represents the radiative part of the source term.

Angular discretization

For DO model, another discretization called angular discretization is needed besides the normally used spatial discretization (the computational grid). The total angular space 4π at any face between the adjacent cells is discretized into discrete non-overlapping solid angles, the centroids of the solid angles are denoted by the direction vector s_j. Each octant is discretized into $N_\theta \times N_\phi$ solid angles. The angles θ and ϕ, as shown in figure 7, are the polar and azimuthal angles respectively. The angular discretization is uniform in that the polar direction is divided into N_θ equal angles, and the azimuthal direction is divided into N_ϕ equal angles. The discretization in this paper is 2 × 2, which means each octant contains 4 solid angles, with a total number of 32 directions on one face.

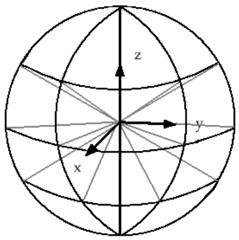

Figure 7. SKETCH MAP OF ANGULAR DISCRETIZATION

The Weighted-Sum-of-Gray-Gases model

The weighted-sum-of-gray-gases model (WSGGM) is a compromise between the totally gray gas model and a complete non-gray model. It is proper and widely used in calculating the radiative heat transfer of the multi-component gas which contains CO_2 and H_2O. The basic assumption of the WSGGM is that the total emissivity over the distance s can be presented as:

$$\varepsilon = \sum_{i=0}^{I} w_{\varepsilon,i}(T)(1-e^{-a_i ps}) \tag{6}$$

where $w_{\varepsilon,i}$ is the emissivity weighting factor for the ith fictitious gray gas, $1-e^{-a_i ps}$ is the ith fictitious gray gas emissivity, a_i is the absorption coefficient of the ith gray gas, p is the sum of the partial pressures of all absorbing gases, and s is the path length. The value of $w_{\varepsilon,i}$ and a_i are obtained from Smith(1982)[10] and Coppalle(1983) [11].

The computational domain and the grid description

The computational domain which contains the whole test section is illustrated in figure 8. Both the hot gas channel and the coolant air channel have extensions on their inlet and outlet. The lengths of the extensions are 0.08m, in which the thermocouples and pitot tubes are located in the test rig.

The grid independence is verified by computing the film cooling of the flat plate with the transparent gas on two grids. The numbers of grid points are 5,501,440 cells and 7,941,120 cells. Both are refined near the surfaces of the plate and the film-cooling holes. The prediction of the temperatures on the two grids are showed in figure 9, with the temperature range from the temperature of the coolant air and that of the hot gas, 400°C ~ 800°C. Based on the verification, the grid with 5,501,440 cells is enough for the computation. The first grid point away from the refined region has a y^+ value less than 1 (showed in figure 10), and the first five grid points have y^+ less than 5.

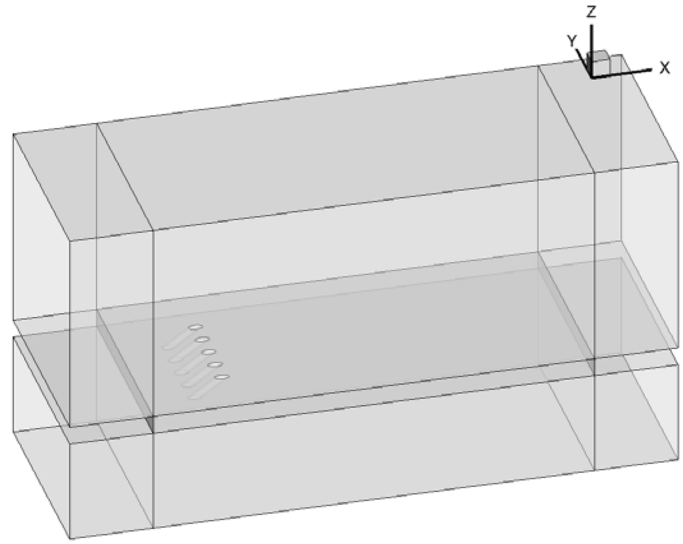

Figure 8. THE ILLUSTRATION OF THE COMPUTATIONAL DOMAIN

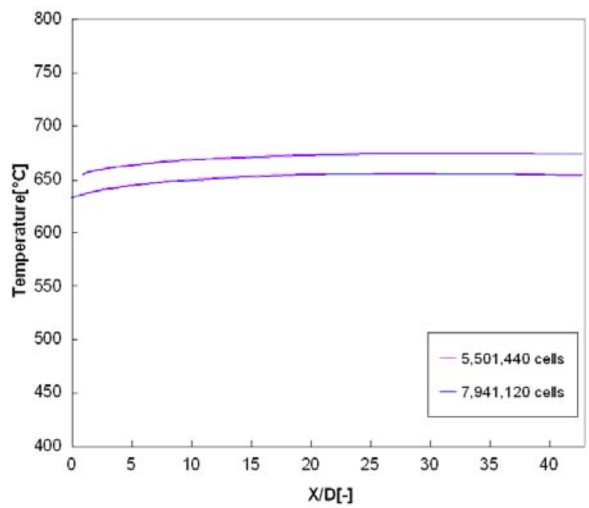

Figure 9. OVERALL COOLING EFFECTIVENESS ALONG THE CENTERLINES OF THE PLATE SURFACES (GRID INDEPENDENCE VERIFICATION)

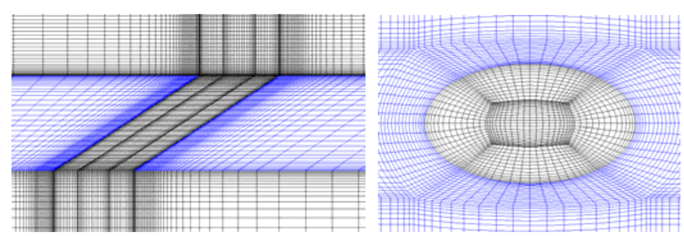

Figure 10. REFINED GRIDS NEAR THE PLATES AND THE FILM COOLING HOLES

Boundary conditions and turbulence model

The mean value of the temperatures and velocities of the inlets and the back pressures of the outlets are acquired from the experiment, which are listed in table 2. The profiles of the temperatures and velocities are calculated from a pre-calculation which includes all the prechannels and the computational domain with no holes. The mass-weighted-average of the temperature and velocity in the no-hole-pre-calculation case at the place which has the same X axis value with the inlets in the five-hole case are required to be close to the data acquired from the experiment.

Table 2. DATA ACQUIRED FROM THE EXPERIMENT

channel	hot gas	coolant air
inlet velocity (m/s)	15.5	10
inlet temperature (°C)	809	416
outlet pressure (Pa)	101403.1	101423.2
mass fraction of CO_2 (%)	6.97	-
mass fraction of H_2O (%)	7.92	-
mass fraction of O_2 (%)	13.73	23.14 (air)
mass fraction of N_2 (%)	balance	76.86 (air)

All the walls are adiabatic except the top and bottom surfaces of the superalloy plate, which are conjugate. The thermal conductivity of the plate varies from 10.4W/m-K to 36.7 W/m-K with the temperature increasing from 15°C to 1500°C[12].

The composition of the fluid at the inlet of the hot gas channel is also acquired from the experiment, as listed in Table 2. The composition of the air of the coolant air inlet is set to the real air composition, according to its name. The properties of each composition are based on the REFPROP program which is an acronym for reference fluid properties[13].

The emissivity of the inlet of the hot gas channel is set to 0.5 due to the combustion, the gas composition and the geometry of the channels ahead of the test section. The plate emissivity is set to 0.8 based on the material. Although the other walls are quartz glass, which is a semi-transparent material, it could be treated as opaque since the whole test section is wrapped by the fiberglass batt. The emissivities of the other walls are set to 1, which is an approximation of the emissivity of fiberglass batt, 0.93~0.96.

The turbulence model used is realizable k-ε with enhanced wall treatment in the near wall region, the SIMPLE algorithm is used to generate solutions. All equations are integrated over each cell of the grid system. The fluxes at the cell faces are interpolated by using second-order upwind differencing.

RESULT

Validation and effect of radiation

Line plots of the temperatures along the centerlines of the plate surfaces (Z = 0 and 18mm, Y = 0) are showed in figure 11. The zero point of the dimensionless x-length is set at the center of the middle film cooling hole outlet. The figure shows that when the radiative heat transfer is taken into account, the numerical temperatures agree well with the experimental ones, which validates the numerical scheme and radiative models. Meanwhile, the temperatures without radiation shows a 10% under-predict, and the temperature difference between the top and bottom centerlines are much smaller than that of the experimental data. It shows that the radiative heat transfer accounts for a large part in the total heat transfer from hot gas side to coolant air side, the radiative heat transfer could not be neglected at the temperature of 800°C.

The temperature distributions on the top and bottom plate surfaces are showed in figure 12 and figure 13. A conclusion can get that besides the great increase in temperature, the temperature distribution is also changed by radiation, especially on the top surface where film cooling take effects. Figure 14 shows when consifering the radiation, the temperature profile on the spanwise direction becomes smoother on both top and bottom surfaces near the film cooling hole, which means the temperature gradient on the spanwise direction caused by the film cooling holes can be decreased by radiation.

On the other side, the flow field is not affected by the radiation(Fig. 15). The reason is that the radiation heat transfer affects the energy equation by source term directly, while its effect on the momentum equation is indirect. The effect must be delivered to the momentum equation by the parameters in the energy equation such as density and pressure, and is greatly weakened during the procedure.

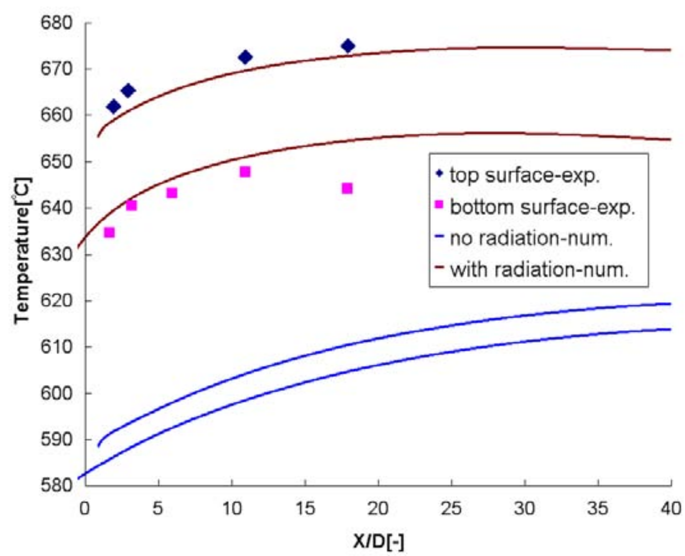

Figure 11. TEMPERATURE ALONG THE CENTERLINES OF THE PLATE SURFACES

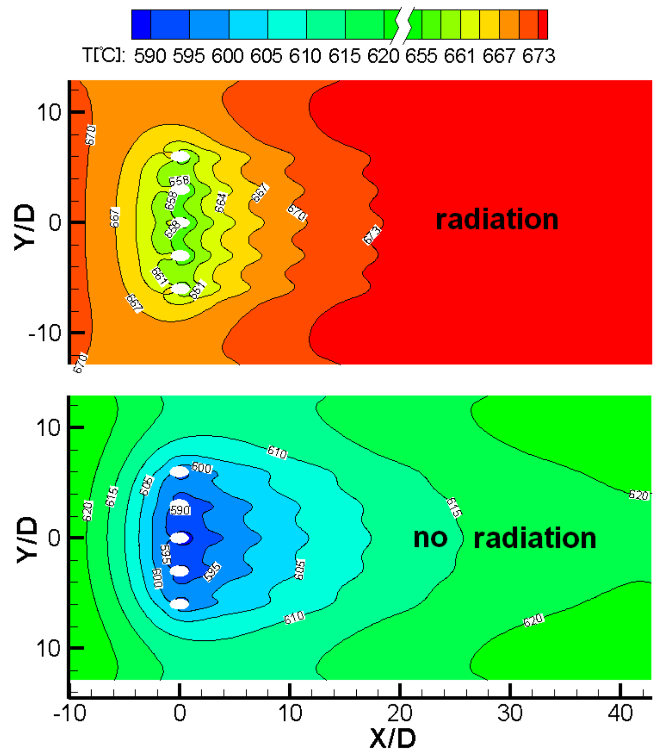

Figure 12. THE TEMPERATURE DISTRIBUTION OF THE TOP PLATE SURFACE (UP: CONSIDERING RADIATION, LOW: NO RADIATION)

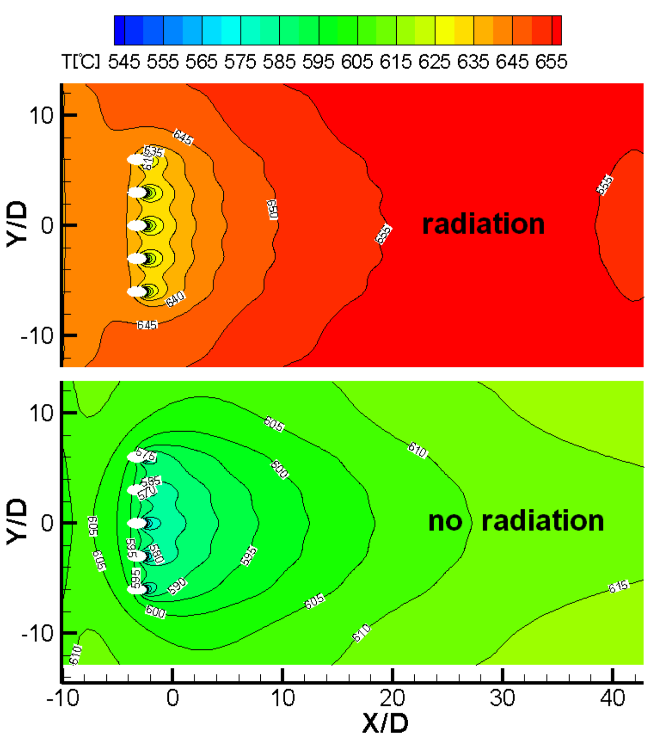

Figure 13. THE TEMPERATURE DISTRIBUTION OF THE BOTTOM PLATE SURFACE (UP: CONSIDERING RADIATION, LOW: NO RADIATION)

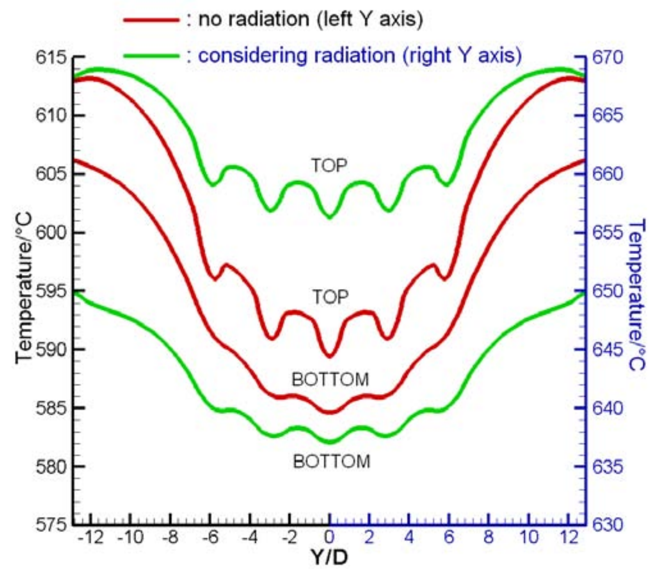

Figure 14. THE SPANWISE TEMPERATURE PROFILE ON THE TOP PLATE SURFACE, X/D = 1

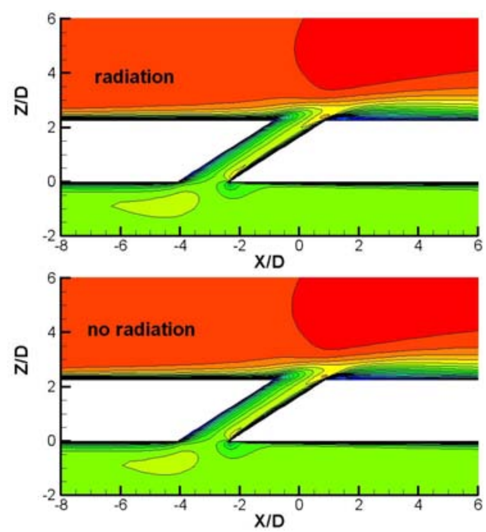

FIGURE 15. VELOCITY FIELD OF THE CENTER PLANE (UP: CONSIDERING RADIATION, LOW: NO RADIATION)

In order to show the radiative effect quantitatively, the overall cooling effectiveness, or the dimensionless temperature Θ, which has the same type of the film cooling adiabatic effectiveness η, is given by:

$$\Theta = \frac{(T_w - T_c)}{T_g - T_c} \tag{6}$$

where T_g, T_c, T_w are the temperatures of the hot gas, the coolant air and the top surface wall. It equals to the film cooling effectiveness when the surface of the plate is adiabatic.

Figure 16 shows line plots of Θ along the centerline of the plate top surface, the adiabatic cases of radiation and no-radiation are employed as the basic, in which the adiabatic cooling effectivenesses η are used.

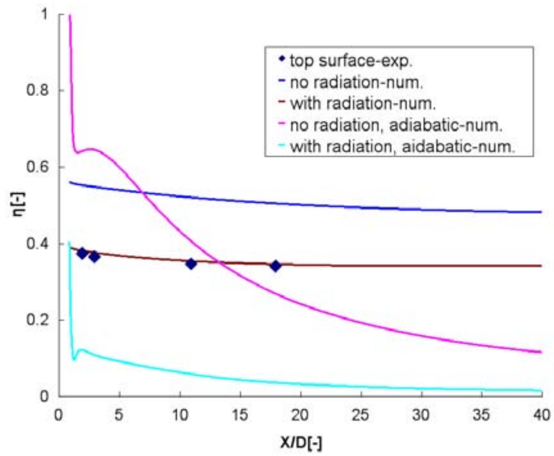

Figure 16. OVERALL / ADIABATIC COOLING EFFECTIVENESS ALONG THE CENTERLINE OF THE TOP PLATE SURFACE

Compares with that of the case with no radiation, the overall cooling effectiveness of the case with radiation is about 0.2 lower, and the decrease of η due to radiation in the adiabatic cases is in an average of 0.4. The decreases of Θ and η shows that the film cooling effect is weakened by radiation greately. On the other hand, it is easy to find out the variation of η along the centerline becomes small by taking radiation into account (decreases 0.43 on temperature variation) and, although not very obvious, the variation of Θ decreases 0.03 as well. So smoothing the temperature can also be caused by radiation.

In the leading edge of the first gas turbine vane with a gas temperature higher than 1200°C (much higher than the condition of the test rig), both high surface temperature and high local temperature gradient will lead to excessive thermal-mechanical load. Since the two effects of radiative heat transfer is contrary, radiation should be treated carefully in high temperature conditions.

Effect of inlet emissivity

In the validation, the emissivity of the inlet of the hot gas channel is set to 0.5 due to the combustion, the gas composition and the geometry of the channels ahead of the test section. At the leading edge of the real first stage gas turbine vane, the internal emissivity is controlled by the same factors, which make the real emissivity changeable. In order to study the effect of the inlet emissivity, some numerical results are discussed.

Figure 17 shows the temperature distributions along the centerline of top plate with different inlet emissivities. It can be seen from the figure that the temperatures along the centerlines on the surfaces increase 3°C when the inlet emissivities increase 0.2, while the temperature difference between the top and bottom centerlines change little. It is easy to understand that the increasing in inlet emissivity leads to the increase of the incident radiation intensity, but has less effect on both convective and radiative heat transfer coefficient while the temperature of the fluid does not change with the inlet emissivity. For the same reason, the temperature distributions on the plate surfaces are not changed by the inlet emissivities except a total increase of 3~4°C(figure 18). The result implicates that the temperature of the first stage gas turbine vane can be prevent from over-high by control the inlet emissivity.

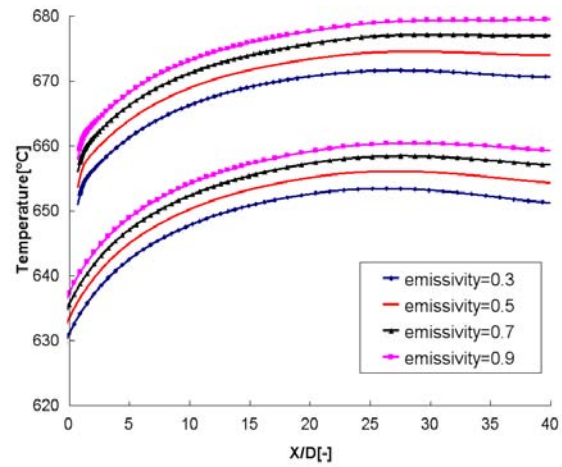

Figure 17. TEMPERATURE ALONG THE CENTERLINES OF THE PLATE SURFACES

SUMMARY

Film cooling system in high temperature gas turbine shows complex characteristics of flow and heat transfer by the interaction of conduction, convection and radiation. In this paper, a film cooling system of a flat plate in high temperature was analyzed. The radiative effects are studied based on the both the experimental and numerical results. The fluid and solid regions were solved simultaneously and DO model was employed into the numerical scheme to solve radiative heat transfer.

Both the results show that when the temperature of the hot gas reaches 800°C, the temperature of the top plate increases about 10% by taking radiation into account. Other two effects of radiation are the great increase of the temperature difference between top and bottom surfaces and the smoother temperature distribution in the spanwise direction when the flow field almost has not been affected by radiation. It shows that the radiation weaken the film cooling effect, but smooth the temperature gradient, which should be considered in designing the film cooling hole in high temperature turbine blade.

Further numerical study on the inlet emissivities shows that the increase in the inlet emissivities will increase the whole temperature of the top plate surface, but have less effect on conductive, convective and radiative heat transfer, which suggests that the control of inlet emissivity is potential for prevent over-high temperature on the first stage gas turbine vane.

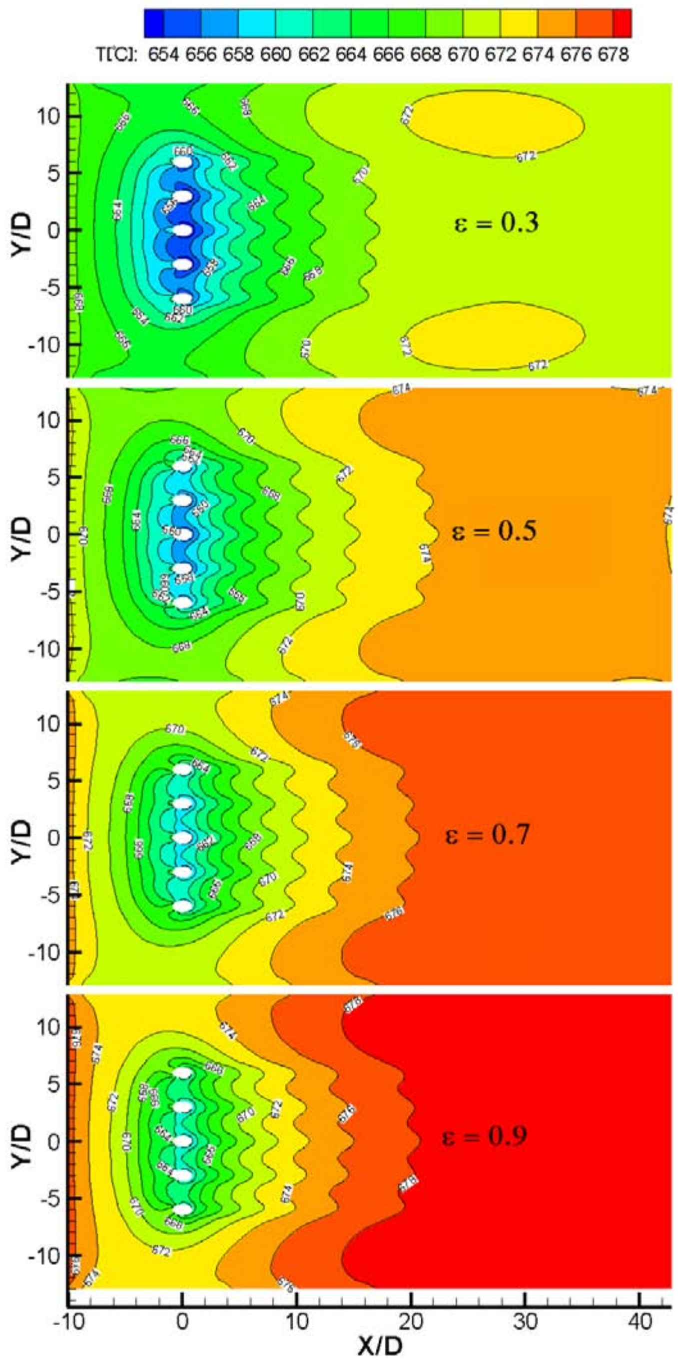

Figure 18. TEMPERATURE DISTRIBUTIONS ON THE TOP SURFACE WITH DIFFERENT INLET EMISSIVITIES

NOMENCLATURE

a	absorption coefficient, m^{-1}
d	diameter of film cooling holes, m
h	heat transfer coefficient: $h = q''/(T_h - T_w)$ on hot gas side and $h = q''/(T_w - T_c)$ on the coolant air side
I	radiation intensity, W/m^2-sr
N_ϕ	number of solid angles in azimuthal direction
N_θ	number of solid angles in polar direction
Nm^3/h	volume flowrate m^3/h at normal condition, i.e., at 0°C, 1atm
n	refractive index
$\vec{n}$	unit surface vector normal pointing out of the domain
q''	heat flux, W/m^2-K
$\vec{r}$	position vector, m
$\vec{s}$	direction vector, m
$\vec{s}'$	scattering direction vector, m
s	path length, m
S_h	source term of the energy equation, W/m^3-sr
T	temperature, °C or K
u_τ	friction velocity: $(\tau_w / \rho_w)^{0.5}$
w	weight factor
X, Y, Z	coordinate system
y^+	$\rho u_\tau y/\mu$, where y is the normal distance from wall

Subscript

c	coolant air
g	hot gas
i	ith fictitious gray gas
j	scattering direction $\vec{s}_j$
w	wall
ε	emissivity

Greek

α	inclination angle
ε	emissivity
Φ	scattering phase function
ϕ	azimuthal angle
μ	dynamic viscosity
Θ	overall cooling effectiveness
θ	polar angle
ρ	density
σ	Stefan-Boltzmann constant (5.672×10^{-8} W/m-K)
σ_s	scattering coefficient, m^{-1}
τ_w	wall shear stress
Ω'	solid angle, sr
ξ_i	direction cosine of the direction vector $\vec{s}$

ACKNOWLEDGEMENTS

The authors would like to acknowledge the financial support from the project supported by National Basic Research Program of China (2007CB210100) and the Project 51076076 supported by National Natural Science Foundation of China.

REFERENCES

[1] Kumar, A., and Kale, S.R., 2002. “Numerical simulation of steady state heat transfer in a ceramic-coated gas turbine blade”. *International Journal of Heat and Mass Transfer*, **45**(24), pp. 4831-4845.

[2] HE Zhi-hong, TAN He-ping, LIU Lin-hua, et al., 2001. “Numerical computation on blade channel radiation in engine”. *Journal of Propulsion Technology*, **22**(01), pp. 65-68, 88.

[3] ZHANG Li-fen , LIU Zhen-xia , LIAN Xiao-chun, 2007. “Numerical study of 3D heat transfer for turbine blade with air cooling”. *Journal of Aerospace Power*, **22**(08), pp. 1268-1272.

[4] Mazzotta, D. W., Chyu, M. K., and Alvin, M. A., 2007. “Airfoil Heat Transfer Characteristics In Syngas And Hydrogen Turbines”. ASME Paper No. GT2007-28296.

[5] Akwaboa, S., Mensah, P. and Diwan, R., 2010. “Effects of Thermal Radiation on Air Plasma Spray (APS) Coated Gas Turbine Blade”. ASME Paper No. GT2010-23660.

[6] Hansmann, T., Wilhelmi, H., and Bohn, D., 1993. “An Experimental Investigation of the Film-Cooling Process at High Temperatures and Velocities”. AIAA Paper No. AIAA-93-5062.

[7] Alvin, M. A., et al., 2010. Materials and Component Development for Advanced Turbine Systems, http://www.netl.doe.gov/.

[8] WANG Wen-ping, ZOU Xin, SUN Peng, et al., 2010. “Experimental and Numerical Investigation on a Flat Plate with Film Cooling”. *Journal of Tsinghua University (Science and Technology)*, **50**(12), pp. 1988-1993.

[9] WANG Wenping, REN Jing, JIANG Hongde, 2010. “Effects of Radiative Heat Transfer on a Highly Thermal Loaded Film Cooled Plate”. Proc. 3rd International Symposium on Jet Propulsion and Power Engineering, Paper No. 2010-ISJPPE-2023.

[10] Smith, T. F., Shen, Z. F., and Friedman, J. N., 1982. “Evaluation of Coefficients for the Weighted Sum of Gray Gases Model”. *Journal of Heat Transfer*, **104**(04), pp. 602-608.

[11] Coppalle, A. and Vervisch, P., 1983. “The Total Emissivities of High-Temperature Flames”. *Combustion and Flame*, **49**, pp. 101-108.

[12] Kermanpur, A., Varahram, N., Davami, P., and Rappaz, M., 2000. “Thermal and Grain-Structure Simulation in a Land-Based Turbine Blade Directionally Solidified with the Liquid Metal Cooling Process”. *Metallurgical and Materials Transactions B*, **31B**(06), pp. 1293-1304.

[13] REFPROP, National Institute of Standards and Technology.

[14] Wang Ping-yang, Tan He-ping, Liu Lin-hua, et al, 2000. “Heat Transfer in Translucent Thermal Barrier Coatings of Turbine Engine”. *Journal of Aerospace Power*, **15**(03), pp. 268-273.

[15] Spuckler, C., 2007. “Effect of an Opaque Reflecting Layer On The Thermal Behavior of a Thermal Barrier Coating”. *Advanced Ceramic Coatings and Interfaces II: Ceramic and Engineering Science Proceedings*, **28**(03), pp. 87-98.

[16] Huang, X., Wang, D., Patnaik, P., Singh, J., 2007. “Design and computational analysis of highly reflective multiple layered thermal barrier coating structure”. *Materials Science and Engineering A*, 2007, 460-461, pp. 101-110.

[17] Na, S., Williams, B., Dennis, R.A., Bryden, K.M., and Shih, T. I-P., 2007. “Internal and Film Cooling of a Flat Plate with Conjugate Heat Transfer”. ASME Paper No. GT2007-27599.

[18] Na, S., Dennis, R.A., Alsup, C., Bryden, K.M., and Shih, T. I-P., 2009. “Effects of Hot-Gas Composition on Temperature Distribution in a Flat Plate Cooled by Internal and Film Cooling”. ASME Paper No. GT2009-59727.

[19] Mazzotta, D. W., Chyu, M. K., Karaivanov, V. G., Slaughter, W. S., and Alvin, M. A., 2008. “Gas-Side Heat Transfer in Syngas, Hydrogen-Fired and Oxy-Fuel Turbines”. ASME Paper No. GT2008-51474.

[20] Siw, S. C., Chyu, M. K., Slaughter, W. S., Karaivanov, V. G., and Alvin, M. A., 2009. “Influence of Internal Cooling Configuration on Metal Temperature Distributions of Future Coal-Fuel Based Turbine Airfoils”. ASME Paper No. GT2009-59829.